

## A MAGNETOHYDRODYNAMIC NONRADIATIVE ACCRETION FLOW IN THREE DIMENSIONS

JOHN F. HAWLEY,<sup>1</sup> STEVEN A. BALBUS<sup>1</sup>, AND JAMES M. STONE<sup>2</sup>

*Submitted to ApJ Letters March 29, 2001*

### ABSTRACT

We present a global magnetohydrodynamic (MHD) three dimensional simulation of a nonradiative accretion flow originating in a pressure supported torus. The evolution is controlled by the magnetorotational instability which produces turbulence. The flow forms a nearly Keplerian disk. The total pressure scale height in this disk is comparable to the vertical size of the initial torus. Gas pressure dominates only near the equator; magnetic pressure is more important in the surrounding atmosphere. A magnetically dominated bound outflow is driven from the disk. The accretion rate through the disk exceeds the final rate into the hole, and a hot torus forms inside  $10 r_g$ . Hot gas, pushed up against the centrifugal barrier and confined by magnetic pressure, is ejected in a narrow, unbound, conical outflow. The dynamics are controlled by magnetic turbulence, not thermal convection, and a hydrodynamic  $\alpha$  model is inadequate to describe the flow. The limitations of two dimensional MHD simulations are also discussed.

*Subject headings:* accretion — accretion disks — instabilities — MHD — black hole physics — X-ray: stars — binaries:

### 1. INTRODUCTION

Observations of underluminous accretion-powered X-ray sources pose a difficulty for accretion theory. The Galactic center is a particularly compelling example: despite the inferred presence of a 2 million solar mass black hole, and the availability of a substantial gas reservoir, only a small fraction of the expected radiation is detected. In a standard Keplerian accretion disk, liberated mechanical energy is promptly radiated, and there is a direct relationship between the accretion rate  $\dot{M}$  and the luminosity  $L$ . A number of alternatives to the standard disk have been put forward, which are classified by the ultimate repository of the orbital energy. In Advection Dominated Accretion Flows (ADAFs, e.g., Narayan & Yi 1994), the energy is retained by the plasma and advected into the hole. In contrast, Blandford & Begelman (1999) proposed that the bulk of the accreting gas and energy might be carried off by a wind. A more recent variation, referred to as Convective Dominated Accretion Flow (CDAF; e.g., Quataert & Gruzinov 2000), brings enhanced viscous heating to the fore, leading to a strong convective flow that stifles the accretion. Since the common feature of all these models is negligible radiative losses, we shall refer to them generically as Non-Radiative Accretion Flows (NRAFs).

Earlier simulations of NRAFs have used several simplifying approximations. Most (e.g., Igumenshchev & Abramowicz 1999, 2000, hereafter IA99, IA00; Stone, Pringle, & Begelman 1999, hereafter SPB) have assumed the flow evolves due to a fortified kinematic viscosity,  $\nu$ . While illuminating some aspects of NRAFs, there are substantial drawbacks to this approach. Most importantly, the results strongly depend upon the specific recipe adopted for  $\nu$ . The origin of angular momentum transport is not unknown, however. It arises from the magnetorotational instability (MRI; Balbus & Hawley 1991), and hydrodynamic and magnetohydrodynamic (MHD) flows have fundamentally different properties.

Stone & Pringle (2001; hereafter SP) include MHD in their

axisymmetric simulations. The stress required to drive the accretion flow emerges self-consistently; it is not a free parameter. But the two-dimensional (2D) restriction is a significant limitation. First, the anti-dynamo theorem (e.g., Moffat 1978) prevents the indefinite maintenance of the poloidal magnetic field in the face of dissipation. Second, axisymmetric simulations tend to over-emphasize the “channel” mode (Hawley & Balbus 1992) which produces coherent internal magnetized flows rather than the more generic MHD turbulence. Consequently, a fully self-consistent NRAF model requires three-dimensional (3D) MHD. In this *Letter* we present and discuss the results of a prototype 3D NRAF simulation.

### 2. THE SIMULATION

The simulation evolves the equations of ideal MHD, i.e., the continuity equation, the induction equation, the Euler equation,

$$\rho \frac{\partial \mathbf{v}}{\partial t} + (\rho \mathbf{v} \cdot \nabla) \mathbf{v} = -\nabla \left( P + Q + \frac{B^2}{8\pi} \right) - \rho \nabla \Phi + \left( \frac{\mathbf{B}}{4\pi} \cdot \nabla \right) \mathbf{B}, \quad (1)$$

and an internal energy equation

$$\frac{\partial \rho \epsilon}{\partial t} + \nabla \cdot (\rho \epsilon \mathbf{v}) = -(P + Q) \nabla \cdot \mathbf{v}. \quad (2)$$

The variables have their usual meanings;  $Q$  is an explicit artificial viscosity (Stone & Norman 1992a), and  $\Phi = -GM/(r - r_g)$  is the Paczyński & Wiita (1980) pseudo-Newtonian potential. We use units with  $GM = r_g = 1$ . The equation of state is adiabatic,  $P = \rho \epsilon (\Gamma - 1)$ , with  $\Gamma = 5/3$ . Radiation transport and losses are omitted. Since there is no explicit resistivity or shear viscosity, the gas can heat only by adiabatic compression, or by the artificial viscosity  $Q$ . We evolve the equations using time-explicit Eulerian finite differencing with the ZEUS algorithms (Stone & Norman 1992a; 1992b; Hawley & Stone 1995; Hawley 2000).

<sup>1</sup>Dept. of Astronomy, University of Virginia, PO Box 3818, Charlottesville, VA 22903, USA. jh8h@virginia.edu; sb@virginia.edu

<sup>2</sup>Dept. of Astronomy, University of Maryland, College Park, MD 20742, USA. jstone@astro.umd.edu

The major difficulties of a 3D simulation include the large number of grid zones needed to resolve an extended spatial domain, and the number of time steps required to evolve the problem over several orbital periods at large radius. In this simulation, we use a somewhat restricted resolution of  $128 \times 32 \times 128$  grid zones in cylindrical coordinates  $(R, \phi, Z)$ . The radial grid extends from  $R = 1.5$  to  $R = 170$ . There are 36 equally-spaced zones inside  $R = 15$ , and 92 zones outside this point that increase logarithmically in size. Similarly, 50  $Z$  zones are equally spaced between  $-10$  and  $10$  with the remainder of the zones logarithmically stretched to the  $Z$  boundaries at  $\pm 60$ . The azimuthal domain is limited to  $\pi/2$ . Hawley (2001) found that reduced angular coverage preserves qualitative features of a simulation with only a small reduction in magnetic energy and stress. The radial and vertical boundary conditions are simple zero-gradient outflow conditions; no flow into the computational domain is permitted. The  $\phi$  boundary is periodic. The magnetic field boundary condition is set by requiring the transverse components of the field to be zero outside the computational domain, while the perpendicular component satisfies the divergence-free constraint.

The prototype simulation starts with a constant specific angular momentum ( $\ell$ ) torus with a pressure maximum at  $r = 100$  (similar to model F of SP) and an inner edge at  $r = 75$ . The initial magnetic field consists of poloidal loops lying along isodensity contours with a volume-averaged energy of  $\beta = P_{\text{gas}}/P_{\text{mag}} = 200$ . The average specific energy of the magnetofluid in the torus is  $-4.6 \times 10^{-3}$  (in units where  $GM = r_g = 1$ ), i.e., it is bound. The simulation is run out to 5 orbits at the initial pressure maximum. This corresponds to 1429 orbits at the marginally stable orbit,  $R = 3$ . The simulation requires over 1.7 million timesteps with an average  $\Delta t = 0.0152$ .

### 3. RESULTS

During the first orbit the field in the torus is amplified by the MRI and by shear, causing the torus to expand. The MRI acts most visibly near the equatorial plane, where the field is predominantly vertical, and the long-wavelength, nearly axisymmetric modes of the MRI grow rapidly. The linear growth phase ends shortly after one orbit, and the magnetic energy has increased to  $\beta \approx 2-10$ .

Over the next orbit, low- $m$  spiral arms of gas accrete from the inner edge of the torus, forming a vertically thin and very nonuniform disk. Strong magnetic fields surround the gas. Due to the initial field topology, a current sheet forms near the equator which proves unstable to vertical oscillations. As more gas leaves the torus, the disk fills out and thickens. Low density material is driven off the forming disk to create a backflow.

As time advances, the initial constant- $\ell$  torus evolves to a nearly Keplerian angular momentum distribution. There is net accretion inside of  $R = 100$ , and net outflow beyond this point. Inside of  $R = 100$  the NRAF forms a modestly thick, nearly Keplerian disk. In the disk, accretion results from MHD turbulence, but the final accretion rate into the black hole need not match the supply rate precisely, and it does not. Because the inflow is hot, geometrically thick, and nearly Keplerian, inflow is difficult past the marginally stable orbit. To accrete the gas must pass through a narrow gap in the centrifugal barrier at the equator. Gas splashes off the centrifugal barrier near the hole, forming a pressure-supported torus and creating a backflow that adds to a growing low density envelope around a higher density Keplerian core.

Between orbits 4 and 5, the disk is well-formed and reasonably steady. Figure 1 is a series of  $(R, z)$  contour plots of azimuthally averaged values at  $t = 5$  orbits showing that most of the gas is located in a modestly thick disk surrounded by a low density, highly magnetized atmosphere. Near the equator gas pressure is dominant, i.e.,  $\beta > 1$ , but in the surrounding region  $\beta < 1$ . The gas pressure scale height is  $H \approx 7-10$ , decreasing rapidly inside  $R = 10$ . The total pressure (gas plus magnetic) is much smoother, and has a scale height  $H \approx 20$  at  $R = 100$  that decreases slowly inward. The gas density, vertically averaged over one gas pressure scale height, is nearly constant from  $R = 50$  down to  $R = 10$ , where it increases rapidly to a peak at  $R = 5.5$ . Inside  $R = 10$ , the disk resembles a pressure supported torus.

The specific angular momentum  $l(R)$  tracks a Keplerian distribution throughout the disk, although in places it is up to 10% below the Keplerian value. The angular velocity  $\Omega$  is constant along cylinders through the main portion of the disk, consistent with  $P = P(\rho)$  there. In hydrodynamic simulations, surfaces of constant entropy  $S$  coincide with those of specific angular momentum  $\ell$ . This corresponds to marginal stability by one of the Høiland criteria. As already noted by SP, with MHD the level surfaces of  $S$  and  $\ell$  do not line up, particularly inside the main disk.

Magnetic fields in the disk produce Maxwell stress, MHD turbulence, and angular momentum transport. Between orbit 4 and 5 the ratio of the vertical- and  $\phi$ -averaged Maxwell stress to the gas pressure ranges from 0.1 to 0.2 inside of  $R = 100$ .

The mass inflow and outflow rates through every cylindrical radius are computed as a function of time. An average over the last orbit shows that these two are nearly equal, although inflow exceeds outflow (Fig. 2). Of course the instantaneous inflow and outflow rates merely represent the flow produced by the MHD turbulent velocity fluctuations. The net accretion rate,  $\dot{M}$ , is due to the resulting drift velocity, which is always considerably smaller.

At the end of the run the total mass on the grid has decreased by 5.4%. Roughly 51% of this leaves through the outer radial boundary, 43% through the upper and lower  $Z$  boundaries, and the remaining 6% is accreted into the black hole. A higher resolution torus simulation (Hawley & Krolik 2001) shows that the magnetic stress can remain large down to and beyond the marginally stable orbit. This effect could increase  $\dot{M}$ , but the present simulation is not sufficiently well-resolved to address this point. The flow through the outer radial boundary is a consequence of the gain in  $\ell$  in the outer part of the torus. The flow through the  $Z$  boundaries is driven from the accretion disk by gas and magnetic pressure. Part of this is an unbound, high temperature hollow conical outflow confined to the axis region by surrounding magnetic pressure. This can be seen in the gas pressure plot of Figure 1. The remainder of the outflow remains bound, although its specific energy is greater than that of the initial torus.

The initial average specific energy for the gas is  $-4.6 \times 10^{-3}$ . At 5 orbits this has decreased to  $-4.9 \times 10^{-3}$  as the gas remaining on the grid becomes more bound. The total thermal, magnetic, poloidal kinetic, and orbital energies of the gas that remains on the grid all increase with time. The magnetic energy has increased the most, receiving 42% of the total net energy increase; 95% of this is in toroidal field. The thermal, orbital and kinetic energies comprise 25%, 21%, and 12% of the increase respectively.

## 4. DISCUSSION

4.1. Comparison with  $\alpha$  models

Full 3D MHD simulations are difficult and expensive; are they necessary? With respect to the hydrodynamical alternative the answer is clearly yes. Such simulations (IA99; SPB; IA00) have shown that the results depend strongly on the magnitude of  $\alpha$  and the form assumed for the stress. Thus, a self-consistent stress is essential for understanding NRAF dynamics.

One should not lose sight of the fact that this is a high Reynolds number turbulent system, not a low Reynolds number laminar flow. For example, the result that large Shakura-Sunyaev  $\alpha$  ( $v = \alpha c_s^2 / \Omega$ ) accretion flows are stable, laminar and accrete fully into the central hole (IA99; IA00) is a literal consequence of using a Navier-Stokes viscosity for the stress. With stress from MHD turbulence  $\alpha \sim 1$  necessarily implies velocity fluctuations with speeds comparable to the sound speed  $c_s$  on scales of order the size of the system.

A second hydrodynamic result is that NRAFs are driven to a state of marginally convective instability (SPB; Quataert & Gruzinov 2000; IA00). This is the basis for CDAF solutions. But this cannot hold in MHD. Recall the form of the Høiland criteria that applies to adiabatic perturbations in *magnetized* flow (Balbus 1995):

$$N^2 + \frac{\partial \Omega^2}{\partial \ln R} > 0 \quad (3)$$

$$-\left(\frac{\partial P}{\partial Z}\right) \left( \frac{\partial \Omega^2}{\partial R} \frac{\partial \ln P \rho^{-5/3}}{\partial Z} - \frac{\partial \Omega^2}{\partial Z} \frac{\partial \ln P \rho^{-5/3}}{\partial R} \right) > 0 \quad (4)$$

where  $N^2 = -(3/5\rho)\nabla P \cdot \nabla \ln P \rho^{-5/3}$  is the Brunt-Väisälä frequency. Note the symmetry between the angular velocity gradients and the entropy gradients, and the absence of any stabilizing epicyclic frequency. At least one of these criteria must always be strongly, not marginally, violated in an accretion flow: this is what is responsible for the existence of the turbulent stress. Convection does not arise *in addition* to this fundamental instability, it is part of the instability that produces the anomalous stress in the first place. In particular, one cannot argue for the marginal stability of a rotationally modified convective process independently of what is called  $\alpha$ . Whatever the sign of the Brunt-Väisälä frequency, the instability is essentially the same one at work in a standard Keplerian disk. Indeed, in contrast to hydrodynamical treatments, we find that the MHD flows show no tendency at all toward marginal stability.

The 3D MHD simulation does show large scale turbulent rolls and outflows qualitatively similar to those reported in small  $\alpha$  hydrodynamic simulations. In the hydrodynamic simulations, however, all the rotational energy released by the stress goes immediately into heat. Some of this heat returns to kinetic energy in the form of large-scale convection. This implies that large-scale shear is converted into heat, producing large-scale convective rolls, which then prevent the accretion process that was driving the heating in the first place. In MHD, the orbital energy goes directly into turbulent kinetic and magnetic energies. The magnetic energy constitutes a particularly important component of the total energy budget. Heating results from dissipation at small scales. In a real plasma, this will depend on microscopic resistivity and viscosity. In the simulation, turbulent rolls are not thermal in origin. More generally the kinetic energy of convective motions is small compared with the dynamical activity associated with MHD instabilities and with the large scale flow itself.

We also remark that in any turbulent flow, the net accretion rate will always be small compared to any locally sampled instantaneous value. As Figure 2 shows, inward and outward accretion rates almost exactly cancel in our purely dynamical simulation. This is not a unique property of inwardly-transported convective energy fluxes. It is a hallmark of turbulence. In both viscous hydrodynamical and MHD treatments, turbulent eddy velocities are much larger than the residual inward drift velocity. It is precisely this ordering that allows the  $\alpha$  formalism for the *mean* flow dynamics to be derived from the equations of motion themselves (Balbus & Papaloizou 1999).

## 4.2. Comparison with 2D MHD models

Next we compare the present simulation with the 2D models of SP. In the equivalent run (SP's Run F), the initial infall phase during orbits 2–3 was relatively smooth and dominated by the channel flow of the MRI. Subsequent evolution was turbulent. In 3D, the initial smooth phase does not occur; the evolution is always turbulent. The 3D flow also generates greater outflow from the disk.

After 3 orbits in both 2D and 3D, the inner regions of the flow are dominated by MHD turbulence driven by the MRI. Interestingly, there appear to be few differences between time- and angle-averaged quantities in either case. For example, comparison of the contours in Fig. 1 with Figure 4 in SP show that both produce a nearly barytropic disk near the midplane with  $\Omega$  contours parallel to cylindrical radii, but with no correlation between the specific angular momentum and entropy. Moreover, the net  $\dot{M}$  values are similar:  $3 \times 10^{-3}$  in 2D versus  $\sim 2 \times 10^{-3}$  in 3D, in units of the initial mass of the torus per orbit at the initial pressure maximum. Radial profiles of time-averaged data in the main disk show many similarities: in both cases  $P_{gas} \sim 10P_{mag}$  and  $v_\phi > c_s > v_{Alfven}$  at all radii (see figure 6 in SP). The most obvious differences between the 2D and 3D models are near the axis, and these are attributable to spherical 2D versus cylindrical 3D inner boundary geometries.

Eventually all axisymmetric models are limited by the antidymano theorem. Toward the end of the SP simulations the turbulence in the initial torus dies down, and remains only in the flow close to the black hole. Higher resolution is possible in 2D, but this only prolongs the duration of the turbulent phase before eventual decline. In addition, the toroidal field MRI cannot be simulated in axisymmetry, which limits 2D models to initial conditions that contain large-scale poloidal field.

## 5. CONCLUSION

We have performed a three-dimensional MHD simulation of an NRAF originating from a constant- $\ell$  torus located at 100 gravitational radii. The resulting flow does not resemble a classical ADAF. Most of the infalling mass and released energy does not end in the hole. In this sense the flow might be better described as an inflow/outflow solution of the type outlined by Blandford & Begelman (1999). The general appearance of the flow is similar to the low- $\alpha$  hydrodynamic models of SPB, IA99 and IA00. Of course this is what one should expect for any hot, rotating, nearly Keplerian accretion flow. We have argued that the CDAF picture is also inappropriate because the classic Høiland criteria do not apply to an MHD flow. The outflow is not driven by thermal convection, but by the action of the same instability that accounts for  $\alpha$ , namely the MRI. Marginally stability is not attained.

We conclude by considering some directions for future work. In the present simulation an internal energy equation is used and the only source of dissipative heating is the artificial viscosity  $Q$ . Some amount of the total energy is inevitably lost in this formulation. A portion of this can be recaptured through artificial resistivity, although this made no significant difference in flow structure or accretion rates when tested in 2D (SP). In any case, a more detailed study of the energy flow in a 3D simulation would be enlightening. Higher resolution is needed in the inner region to capture the details of the inner disk boundary and the flow past the marginally stable orbit. Models with a greater radial domain would allow the inflow to proceed over several decades in distance and to liberate greater amounts of gravitational energy. High-resolution axisymmetric MHD sim-

ulations can play an important role here in mapping out the types of flows that are possible. Longer evolutions would provide greater confidence that the results have lost memory of the initial conditions, but, because of the antidynamo theorem, true steady states can only be obtained in 3D.

JFH and SAB acknowledge support under NSF grant AST-0070979, and NASA grants NAG5-9266, NAG5-7500, and NAG5-106555. JMS acknowledges support under NASA grant NAG5-3836. The simulation was carried out on the IBM Blue-horizon system of the San Diego Supercomputer Center of the National Partnership for Advanced Computational Infrastructure, funded by the NSF.

## REFERENCES

- Balbus, S. A. 1995, *ApJ*, 453, 380  
 Balbus, S. A., & Hawley, J. F. 1991, *ApJ*, 376, 214  
 Balbus, S. A., & Papaloizou, J. C. B. 1999, *ApJ*, 521, 650  
 Blandford, R. D., & Begelman, M. C. 1999, *MNRAS*, 303, L1  
 Hawley, J. F. 2000, *ApJ*, 528, 462  
 Hawley, J. F. 2001, *ApJ*, 553, in press  
 Hawley, J. F., & Balbus, S. A. 1992, *ApJ*, 400, 595  
 Hawley, J. F., & Krolik, J. H. 2001, *ApJ*, 548, 348  
 Hawley, J. F., & Stone, J. M. 1995, *Comp Phys Comm*, 89, 127  
 Igumenshchev, I. V., & Abramowicz, M. A. 1999, *MNRAS*, 303, 309 (IA99)  
 Igumenshchev, I. V., & Abramowicz, M. A. 2000, *ApJS*, 130, 463 (IA00)  
 Moffat, K. 1978, *Magnetic Field Generation in Electrically Conducting Fluids* (Cambridge University Press: Cambridge)  
 Narayan, R. & Yi 1994, *ApJ*, 428, L13  
 Paczyński, B., & Wiita, P. J. 1980, *A&A*, 88, 23  
 Quataert, E. & Gruzinov, A. 2000, *ApJ*, 539, 809  
 Stone, J. M., & Norman, M. L. 1992a, *ApJS*, 80, 753  
 Stone, J. M., & Norman, M. L. 1992b, *ApJS*, 80, 791  
 Stone, J. M., & Pringle, J. 2001, *MNRAS*, 322, 461 (SP)  
 Stone, J. M., Pringle, J. E., & Begelman, M. C. 1999, *MNRAS*, 310, 1002 (SPB)

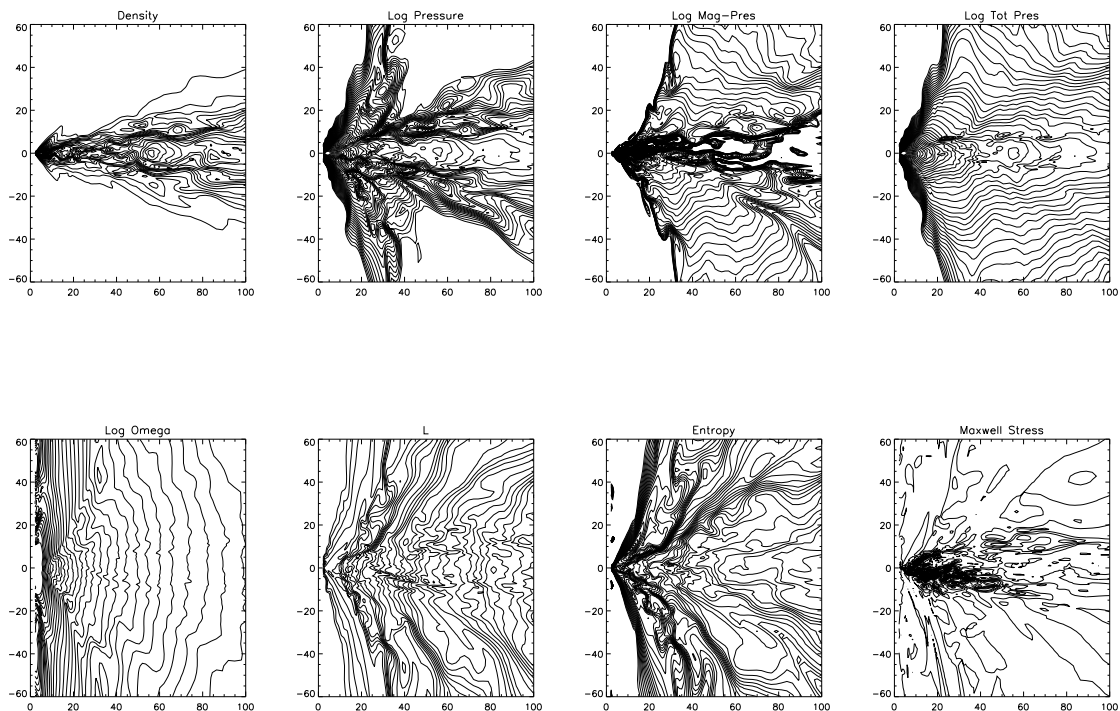


FIG. 1.— Azimuthally-averaged contour plots of indicated quantities in the inner region of the computation at  $t = 5$  orbits. Plots are gas density, log of the gas pressure, log of the magnetic pressure, log of the total pressure, log of the angular velocity  $\Omega$ , specific angular momentum  $\ell$ , the entropy,  $S = \ln(P/\rho^{5/3})$ , and the Maxwell stress,  $T_{R\phi} = -B_R B_\phi / 4\pi$ .

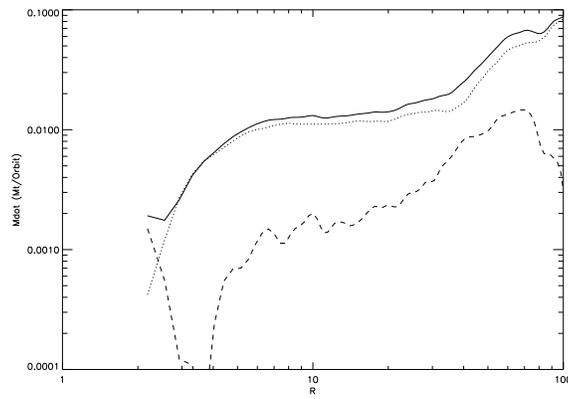


FIG. 2.— Amplitude of the total mass inflow rate (solid line), mass outflow rate (dotted line), and net accretion rate (dashed line) through cylindrical radius  $R$ , averaged in time between orbit 4 and 5.